

A numerical solution for the electromagnetic scattering by a two-dimensional inhomogeneity

K. H. Lee* and H. F. Morrison†

ABSTRACT

A numerical solution for electromagnetic scattering from a two-dimensional earth model of arbitrary conductivity distribution has been developed and compared with analog model results. A frequency-domain variational integral is Fourier transformed in the strike direction, and a solution is obtained using the finite-element method for each of a finite number of harmonics or wavenumbers in transform space. The solution is obtained in terms of the secondary electric fields. Principally due to the inaccuracy associated with numerical derivatives of electric fields, the secondary magnetic field is computed by integrating over the scattering currents in harmonic space and is then inverse Fourier transformed.

INTRODUCTION

An important class of electromagnetic (EM) methods used in exploration geophysics is that which uses sources of finite dimension such as current loops or grounded wires. Used mainly for detection of discrete conductors such as massive sulfide ore deposits, a wide variety of both time- and frequency-domain ground and airborne dipole systems have been discussed (Ward, 1980). Interpretation of the data from surveys using these systems has generally relied on theoretical solutions, using either simple models in free space or scale-model results, again often in free space. For many exploration problems, especially in areas with host rocks of high resistivity, the free-space models have been effective for interpretation. When greater depth of exploration is required, through conductive surface layers or in conductive host rock, a much more accurate interpretation is required. Such interpretations must account for the shielding effects of the surroundings, and for the current gathering, or channeling effects of the conductive target on the induced currents in the host rock or overburden.

Considerable insight into some of these problems has been gained with a series of model studies using a finite, thin, rectangular plate either in free space (Annan, 1974), under a con-

ductive overburden (Lajoie and West, 1976), or more recently, in a conductive host and under a surface layer (Weidelt, 1981; Hanneson, 1981).

Another model which has met with some success in the three-dimensional (3-D) finite conductor, usually a rectangular block, in a conductive host and with a surface layer. Such solutions by Hohmann (1975), Weidelt (1975), Meyer (1977), Pridmore (1978), and Lee et al. (1981) are useful for simple, confined conductors at frequencies for which the dimensions of the body are on the order of the skin depth. For complex shapes or for higher frequencies the computing costs become prohibitive even on the largest computers.

Geologic models in which the electrical parameters are invariant in the strike direction also constitute an important class of targets in EM exploration. They are particularly appropriate for dipole methods because the fields fall off so rapidly from the source that an elongated target may be satisfactorily represented by a two-dimensional (2-D) equivalent. Such a representation is often not valid for line sources or for plane-wave inducing fields.

A detailed discussion of the finite-element method using the variational principle was given by Coggon (1971), and subsequently a finite-element formulation for the case of a dipole source over a 2-D conductivity distribution was offered by Ryu (1971). Since magnetic fields are continuous in a region without magnetic susceptibility contrasts, the problem was formulated initially in terms of unknown magnetic fields. The equations were Fourier transformed in the strike direction y , and solutions for a 2-D model were obtained as a function of wavenumber in the strike direction. Inverse transformations then yield the solution in x , y , and z . There are numerical difficulties with this approach caused by rapid changes of the gradients of the magnetic field near the earth-air interface. Lee (1978) reformulated the problem in terms of electric fields and succeeded in obtaining solutions for some simple models. Stoyer and Greenfield (1976) published a finite-difference solution using a coupled transmission sheets analogy.

The accuracy of these numerical solutions has been in doubt because there was nothing to which they could be compared. In

Manuscript received by the Editor May 16, 1984; revised manuscript received September 14, 1984.

*Earth Science Division, Lawrence Berkeley Laboratory, University of California, Berkeley, CA 94720.

†Engineering Geosciences, University of California, Berkeley, CA 94720.

© 1985 Society of Exploration Geophysicists. All rights reserved.

the present study we have analyzed the numerical solutions at length, tested a variety of algorithms, and most importantly, compared the numerical results to scale-model results. For the range of frequencies and parameters for which the solution is valid, the resulting program has been useful in analyzing a number of important exploration problems.

FORMULATION OF THE VARIATIONAL INTEGRAL

Using Maxwell's equations,

$$\nabla \times \mathbf{E} = -\frac{\partial \mathbf{B}}{\partial t}, \quad (1)$$

and

$$\nabla \times \mathbf{H} = \mathbf{J} + \frac{\partial \mathbf{D}}{\partial t}, \quad (2)$$

and the constitutive relations and Ohm's law, i.e.,

$$\mathbf{B} = \mu \mathbf{H}, \quad (3)$$

$$\mathbf{D} = \epsilon \mathbf{E}, \quad (4)$$

and

$$\mathbf{J} = \sigma \mathbf{E} \quad (5)$$

Stratton (1941) showed that

$$-\int_S \mathbf{E} \times \mathbf{H} \cdot \mathbf{n} \, ds = \int_v \sigma \mathbf{E} \cdot \mathbf{E} \, dv + \frac{\partial}{\partial t} \int_v \left[\frac{\epsilon}{2} \mathbf{E} \cdot \mathbf{E} + \frac{\mu}{2} \mathbf{H} \cdot \mathbf{H} \right] dv, \quad (6)$$

where \mathbf{n} is a unit vector outward normal to the surface S enclosing v (Figure 1). Integrating the right-hand side of equation (6) in time and adding the source energy due to a current source \mathbf{J}_s , we can write the total EM energy I , contained in v as,

$$I(\mathbf{E}) = \int_v \left[\frac{k^2}{2\omega^2\mu} \mathbf{E} \cdot \mathbf{E} - \frac{1}{2\omega^2\mu} (\nabla \times \mathbf{E}) \cdot (\nabla \times \mathbf{E}) + \frac{1}{j\omega} \mathbf{E} \cdot \mathbf{J}_s \right] dv. \quad (7)$$

The variational integral is written in terms of \mathbf{E} and a time dependence $e^{j\omega t}$ is used. The propagation constant is given by

$$k = (\omega^2\mu\epsilon - j\sigma\omega\mu)^{1/2}.$$

The stationary principle (Morse and Feshbach, 1953) imposed on the variational integral [equation (7)] results in the following vector wave equation for the electric field \mathbf{E} :

$$k^2 \mathbf{E} - \nabla \times \nabla \times \mathbf{E} = j\omega\mu \mathbf{J}_s, \quad (8)$$

thus confirming the correct \mathbf{E} field behavior in v .

The presence of a finite source \mathbf{J}_s , a grounded electric dipole, or a loop of wire of finite radius often creates numerical problems simply because it is difficult to integrate. This can be easily avoided by using the principle of superposition to write \mathbf{E} in terms of a primary part \mathbf{E}^p and a secondary part \mathbf{E}^s , i.e.,

$$\mathbf{E} = \mathbf{E}^p + \mathbf{E}^s, \quad (9)$$

and substituting into the variational integral $I(\mathbf{E})$. Then,

$$I(\mathbf{E}^p + \mathbf{E}^s) = \int_v \left\{ \frac{k^2}{2\omega^2\mu} (\mathbf{E}^p + \mathbf{E}^s) \cdot (\mathbf{E}^p + \mathbf{E}^s) - \frac{1}{2\omega^2\mu} [\nabla \times (\mathbf{E}^p + \mathbf{E}^s)] \cdot [\nabla \times (\mathbf{E}^p + \mathbf{E}^s)] + \frac{1}{j\omega} (\mathbf{E}^p + \mathbf{E}^s) \cdot \mathbf{J}_s \right\} dv. \quad (10)$$

Taking the variation of the right-hand side of equation (10) with respect to \mathbf{E}^s , we find

$$\begin{aligned} \delta I(\mathbf{E}^p + \mathbf{E}^s) = & \delta \int_v \left[\frac{k^2}{2\omega^2\mu} \mathbf{E}^p \cdot \mathbf{E}^p - \frac{1}{2\omega^2\mu} (\nabla \times \mathbf{E}^p) \right. \\ & \times (\nabla \times \mathbf{E}^p) + \left. \frac{1}{j\omega} \mathbf{E}^p \cdot \mathbf{J}_s \right] dv \\ & + \delta \int_v \left[\frac{k_b^2}{\omega^2\mu} \mathbf{E}^p \cdot \mathbf{E}^s - \frac{1}{\omega^2\mu} (\nabla \times \mathbf{E}^p) \right. \\ & \times (\nabla \times \mathbf{E}^s) + \left. \frac{1}{j\omega} \mathbf{E}^s \cdot \mathbf{J}_s \right] dv \\ & + \delta \int_v \left[\frac{k^2}{2\omega^2\mu} \mathbf{E}^s \cdot \mathbf{E}^s - \frac{1}{2\omega^2\mu} (\nabla \times \mathbf{E}^s) \right. \\ & \times (\nabla \times \mathbf{E}^s) + \left. \frac{\Delta k^2}{\omega^2\mu} \mathbf{E}^p \cdot \mathbf{E}^s \right] dv, \end{aligned} \quad (11)$$

where Δk^2 is the square of the propagation constant of the actual medium subtracted from the square of the propagation constant k_b of the background medium for which the primary field \mathbf{E}^p is computed. The first term on the right-hand side of equation (11) vanishes since the integral is independent of \mathbf{E}^s . Applying the vector identity,

$$\nabla \cdot \mathbf{A} \times \mathbf{B} = \mathbf{B} \cdot \nabla \times \mathbf{A} - \mathbf{A} \cdot \nabla \times \mathbf{B},$$

and the divergence theorem, the second term becomes

$$\begin{aligned} \int_v \frac{1}{\omega^2\mu} [k_b^2 \mathbf{E}^p - \nabla \times \nabla \times \mathbf{E}^p - j\omega\mu \mathbf{J}_s] \cdot \delta \mathbf{E}^s \, dv \\ + \int_S \frac{1}{\omega^2\mu} \nabla \times \mathbf{E}^p \times \delta \mathbf{E}^s \cdot \mathbf{n} \, ds. \end{aligned}$$

The volume integral is identically zero since the integrand is always zero. Assuming that the secondary electric field is pre-

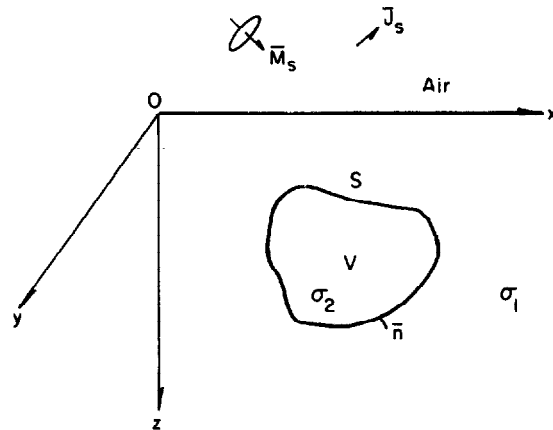


FIG. 1. A general geophysical EM system.

scribed on S , the surface integral also vanishes. Hence the effective variational integral for the secondary field is

$$I(\mathbf{E}^s) = \int_v \left[\frac{k^2}{2\omega^2\mu} \mathbf{E}^s \cdot \mathbf{E}^s - \frac{1}{2\omega^2\mu} (\nabla \times \mathbf{E}^s) \cdot (\nabla \times \mathbf{E}^s) + \frac{\Delta k^2}{\omega^2\mu} \mathbf{E}^p \cdot \mathbf{E}^s \right] dv. \quad (12)$$

The current source \mathbf{J}_s has been removed from the integral. As a result, it can be shown that the variation of $I(\mathbf{E}^s)$, with a proper boundary condition satisfied, leads to the wave equation

$$k^2 \mathbf{E}^s - \nabla \times \nabla \times \mathbf{E}^s = -\Delta k^2 \mathbf{E}^p. \quad (13)$$

One can derive the same equation directly from Maxwell's equations by initially decomposing the fields into the primary and secondary parts.

HARMONIC VARIATIONAL INTEGRAL

If the medium of interest is two-dimensional, we can reduce the variational integral [equation (12)] to a 2-D problem in harmonic space using a Fourier transformation. To begin, we chose a magnetic dipole source oriented in the direction perpendicular to the strike. With reference to Figure 1, it is assumed that the strike is parallel to the y -axis. Using the Fourier integral and appropriate symmetry conditions, we can write

$$P(x, y, z) = \frac{1}{\pi} \int_0^\infty \hat{P}(x, k_y, z) \cos k_y y \, dk_y, \quad (14-1)$$

and

$$Q(x, y, z) = \frac{j}{\pi} \int_0^\infty \hat{Q}(x, k_y, z) \sin k_y y \, dk_y, \quad (14-2)$$

where P and Q represent field components which are symmetric and asymmetric in y , respectively. Instead of directly substituting these Fourier integrals into the variational integral, we may first approximate them by

$$P(x, y, z) = \frac{1}{L} \sum_{i=0}^N \hat{P}(x, \eta_i, z) \cos \eta_i y, \quad (15-1)$$

and

$$Q(x, y, z) = \frac{j}{L} \sum_{i=1}^N \hat{Q}(x, \eta_i, z) \sin \eta_i y, \quad (15-2)$$

where $\eta_i = \pi(i/L)$, $i = 0, 1, \dots, N$, and it is assumed that field quantities are periodic in y with a period of $2L$. Upon substituting equations (15) into the variational integral and carrying out integration along y from $-L$ to L , we find

$$I(\mathbf{E}^s) = I_0(\mathbf{E}_0^s) + \sum_{i=1}^N I_i(\mathbf{E}_i^s), \quad (16)$$

where after dropping (x, η_i, z) ,

$$\begin{aligned} I_i(\mathbf{E}_i^s) = & \frac{1}{L} \int_s \frac{1}{2\omega^2\mu} \left[k^2(-E_x^{s2} + E_y^{s2} - E_z^{s2}) \right. \\ & - \left(j\eta_i E_z^s - \frac{\partial E_y^s}{\partial z} \right)^2 + \left(\frac{\partial E_x^s}{\partial z} - \frac{\partial E_z^s}{\partial x} \right)^2 \\ & - \left(\frac{\partial E_y^s}{\partial x} - j\eta_i E_x^s \right)^2 + 2\Delta k^2(-E_x^p E_x^s \\ & \left. + E_y^p E_y^s - E_z^p E_z^s) \right] dx \, dz, \end{aligned} \quad (17)$$

and $I_0(\mathbf{E}_0^s)$ is the zero harmonic variational integral in which the electric field is polarized only in the direction parallel to the strike.

FORMULATION OF THE FINITE-ELEMENT EQUATION

The 2-D model cross-section is simulated by a rectangular mesh. The unknown electric fields are then sequentially assigned to each node. Using a bilinear basis function, the electric field within a rectangular element is written in terms of yet-to-be-determined electric fields at four corner nodes. Thus, each scalar component of the electric fields is given by

$$E^s = \sum_{j=1}^4 N_j E_j^s, \quad (18)$$

where N_j is a shape function (Zienkiewicz, 1977) and E_j^s is the unknown electric field at the j th node of the element. Substituting equation (18) into the variational integral and performing integrations over the region covered by the mesh, we obtain the following approximation to the i th harmonic variational integral:

$$I_i(\mathbf{E}_i^s) = \frac{1}{2} \mathbf{E}^{sT} \mathbf{K} \mathbf{E}^s + \mathbf{E}^{sT} \mathbf{K}_s \mathbf{E}^p, \quad (19)$$

where \mathbf{K} is the total system matrix for \mathbf{E}^s , and \mathbf{K}_s is the source matrix. Following the variational principle, the condition for which the variational integral becomes stationary, we find from equation (19) that

$$\mathbf{K} \mathbf{E}^s + \mathbf{S} = 0, \quad (20)$$

where the vector \mathbf{S} represents $\mathbf{K}_s \mathbf{E}^p$. With the secondary electric field prescribed at the boundary of the 2-D model cross-section, equation (20) may be partitioned into

$$\begin{bmatrix} K_{ii} & K_{ib} \\ K_{bi} & K_{bb} \end{bmatrix} \begin{bmatrix} E_i^s \\ E_b^s \end{bmatrix} = \begin{bmatrix} S_i \\ S_b \end{bmatrix}, \quad (21)$$

where the subscript i indicates that the variable attached to it is defined inside the boundary and the subscript b is for variables on the boundary. The boundary of the 2-D cross-section is placed far from the lateral inhomogeneity. Therefore it is assumed that the secondary field at the boundary is zero. Then the harmonic secondary electric field may be obtained by solving the upper portion of the partitioned matrix equation (21) i.e.,

$$K_{ii} E_i^s = -K_{ib} E_b^s + S_i. \quad (22)$$

The solution to equation (22) implicitly assumes that the secondary electric field is continuous everywhere. However, since the current must be continuous, the electric field normal to an internal boundary between elements of different conductivities is discontinuous. Consider an arbitrary boundary separating elements of different conductivities σ_1 and σ_2 . Then, by Ohm's law and the principle of superposition, the normal component of currents satisfies

$$\hat{y}_1 (E_1^p + E_1^s) = \hat{y}_2 (E_2^p + E_2^s), \quad (23)$$

where $\hat{y}_i = \sigma_i + j\omega\epsilon_i$. Hence, the normal component of the secondary electric fields at one side of the boundary can be explicitly written in terms of the other side, i.e.,

$$E_2^s = \left(\frac{\hat{y}_1}{\hat{y}_2} E_1^p - E_2^p \right) + \frac{\hat{y}_1}{\hat{y}_2} E_1^s. \quad (24)$$

This relation can be easily implemented in the finite-element equations. Suppose that E_1^s is chosen to represent the normal component of electric fields at a particular inhomogeneous node. Then when we formulate the electric field within the element of conductivity σ_2 , the normal component of electric field E_2^s may be replaced by the right-hand side of equation (24). As a result, the solution to the finite-element equations contains E_1^s .

NUMERICAL RESULTS

The 2-D earth is simulated by a mesh consisting of finite rectangular elements of varying conductivity. The size of the mesh is of primary importance, because it dictates the accuracy of the numerical solution. Due to the limitations of the affordable computer, a mesh size of 55×18 nodes, Figure 2, has been used for all the models presented here. The mesh generates the system matrix \mathbf{K} of order 2 970 with half-bandwidth of 60. A symmetric triangular decomposition technique (Reid, 1972) is used to solve the system matrix for the secondary electric field. In this technique one ignores sparsity within the bandwidth and performs no interchanges.

In order to calculate magnetic fields in harmonic (k_y) space, we first employ the simplest technique in which the necessary derivatives of electric fields are numerically obtained and substituted into $\nabla \times \mathbf{E}$. The next step is to inverse transform these secondary harmonic fields using the Fourier integrals given by equation (14). The harmonic field is interpolated by a number of piece-wise quadratic functions in wavenumber space. Then the Fourier integral may be approximated by

$$P(x, y, z) = \frac{1}{\pi} \sum_i \int_{\ell_i}^{u_i} \hat{P}(x, k_y, z) \cos k_y y dk_y, \quad (25a)$$

and

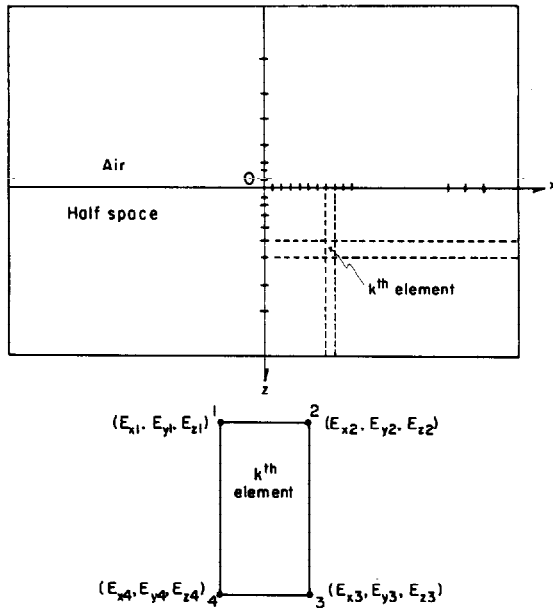


FIG. 2. A finite-element grid and notations used for the description of a rectangle.

$$Q(x, y, z) = \frac{j}{\pi} \sum_i \int_{\ell_i}^{u_i} \hat{Q}(x, k_y, z) \sin k_y y dk_y, \quad (25b)$$

where $\ell_i = \eta_{2i-1}$, $u_i = \eta_{2i+1}$, with $\eta_1 = 0$.

The number of piece-wise integrations has been typically 7, which requires 15 harmonic solutions.

To test the numerical technique, we computed results for a simple model used in scale-model studies of an airborne prospecting system at the University of California, Berkeley. The scale model, Figure 3, represents a vertical slab 12 m wide, 60 m high, and approximately 1.0 km in strike. The slab was $2.63 \Omega \cdot \text{m}$, and it was placed in a half-space of $100 \Omega \cdot \text{m}$. The response was obtained for a coaxial helicopter boom system in which the transmitter and receiver were separated by 12 m and the boom was flown over the target at a height of 20 m from the surface of the half-space, in a direction perpendicular to the strike. The results for the real and imaginary responses at 32 Hz in parts per million (ppm) are shown in the curves in Figure 3. The agreement between the scale model and numerical results is good for the quadrature response; the peak of the anomaly is about 15 percent below the analog result. It is quite possible that the measured resistivity of the model could be in error by 10 percent, and therefore it could be partially responsible for the difference.

The real response, however, is erratic and differs from the tank model result completely. The problem lies in the computation of the magnetic field for which the numerical derivatives (differences) of the electric fields were used. To illustrate the numerical difficulty, we have computed magnetic fields analyti-

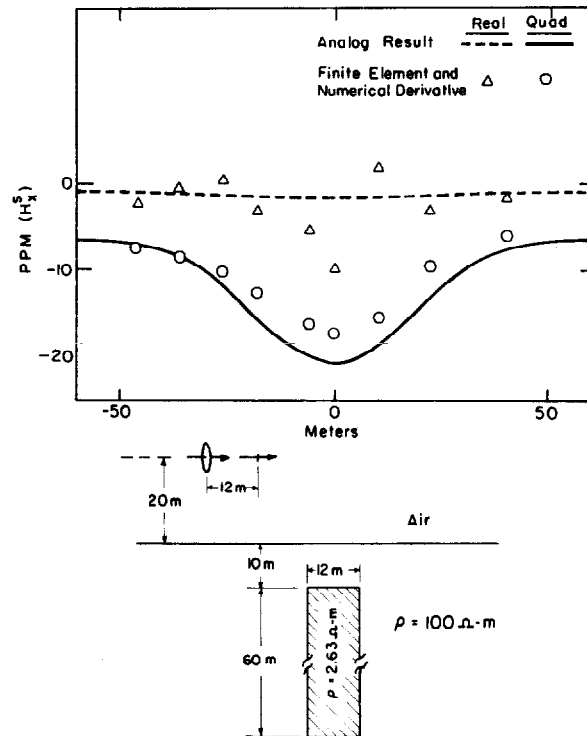
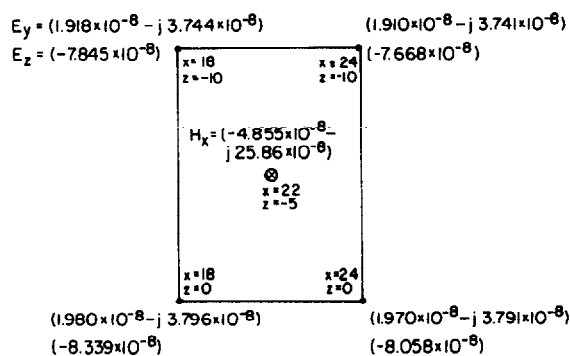


FIG. 3. Numerical model result with the use of numerical derivative. The abscissa represents the location of the array center with respect to the center of the body. The ordinates are in parts per million (ppm) to the free space field.

Table 1. Display of harmonic fields in a rectangle for $k_y = 0.0005 \text{ m}^{-1}$.

cally over a simple half-space and comparisons are made to those numerically obtained.

The electric fields in transformed, harmonic, space over a half-space can be calculated analytically (Lee, 1978) at the four corners of a hypothetical finite-element rectangle. The magnetic field may be computed numerically from $\nabla \times \mathbf{E}$ at the center of the rectangle. This can be compared with the true magnetic field computed analytically at the same point.

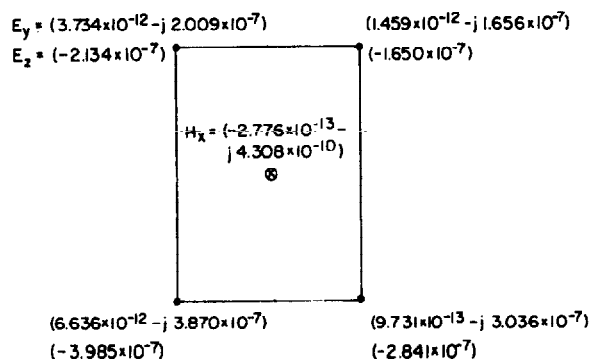
For this example we selected the same half-space ($100 \Omega \cdot \text{m}$) in which the conductive vertical slab was modeled. A horizontal magnetic dipole of moment unity is located at $x = 0, 20 \text{ m}$ above the surface. Using the same frequency of 32 Hz , we calculated the secondary electric fields at four corner nodes of a rectangle in the air. For a wavenumber of $k_y = 0.0005 \text{ m}^{-1}$ these fields are shown schematically in Table 1. Notice that H_x is analytically obtained and displayed at the center of the rectangle. With the assumption that the electric field would behave linearly within the rectangle, one can numerically compute the secondary magnetic field H_x as

$$H_x = \frac{j}{\omega \mu} \left[j k_y E_z - \frac{\partial E_y}{\partial z} \right]$$

$$= (-4.851 - j 25.88) \times 10^{-8} \text{ A/m}.$$

The numerical result is remarkably close to the one analytically computed. However, as the wavenumber increases, this agreement disappears. At $k_y = 0.0625 \text{ m}^{-1}$, the field diagram becomes that given as Table 2.

At this frequency the real part of the H_x is negligible as is shown at the center of the rectangle (Table 2). By taking the numerical derivatives of the electric fields, the horizontal component of the magnetic fields is readily obtained as $H_x = (1.566 \times 10^{-6} - j 5.101 \times 10^{-10}) \text{ A/m}$. There is virtually no imaginary part for E_z ; therefore, the imaginary part of the numerical H_x comes from the vertical derivative of the real part of the electric field E_y . For $k_y \gg |k|$, the field behaves as $e^{-k_y \rho}$, where ρ is the distance on the x - z plane. Over a vertical distance of 10 m the electric field amplitude would decrease by approximately 50 percent ($= e^{-0.625}$) away from the surface of the earth. Consequently, the numerical derivative of the electric field itself generates considerable amount of error. In our example the imaginary part of the numerically computed H_x is about 20 percent larger than the analytically obtained one. The real part of the H_x comes from the difference between the cross-

Table 2. Display of harmonic fields in a rectangle for $k_y = 0.0625 \text{ m}^{-1}$.

derivatives of electric fields E_y and E_z . With a 20 percent numerical error associated with each of the derivatives, the error contained in the difference would be cumulative. As a result the enhanced error itself would become the real part of the numerical solution because the true solution has negligible real part when the harmonic number (k_y) is large.

Although this illustration uses the field from a uniform half-space, similar numerical errors would be expected for numerical derivatives, and their differences, of the scattered electric field from an inhomogeneity. One of the immediate consequences of the analysis is shown in Figure 3. Unfortunately, the problem is fundamental since computationally it is not practical to decrease the element dimensions to increase the accuracy of the derivative at large k_y values.

One way of minimizing this type of numerical error is to obtain the magnetic field from an integral over the currents in the half-space rather than from the derivatives at a point. Assuming that the lateral inhomogeneity is of finite extent, the secondary magnetic field may be obtained by

$$\mathbf{H}^s(x, k_y, z) = \int_s \mathbf{G}^{\text{HJ}}(x, x', k_y, z, z') \times \mathbf{J}^s(x', k_y, z') dx' dz' \quad (26)$$

where \mathbf{G}^{HJ} is the dyadic Green's function for the magnetic field in transform space ($y \rightarrow k_y$; Lee, 1978) and the "scattering current" \mathbf{J}^s is given by (Harrington, 1961)

$$\mathbf{J}^s = \Delta \sigma \mathbf{E}.$$

The scattering current is nonzero only at places where the conductivity of the inhomogeneity σ_a is different from the background conductivity σ_b .

$$\Delta \sigma = \sigma_a - \sigma_b.$$

Using the integral (26) for the magnetic field computation, two important internal checks have been made for the numerical solution. Figures 4a and 4b show the convergence test and a check for the reciprocity principle, respectively, over the model discussed earlier. The convergence test was made by varying the number of cells used for the vertical slab in the finite element solution. Except for the slight oscillation near the center of the profile, the numerical solutions converge to the analog result. The number of cells used for the test were 4, 8, and 18, and the frequency was 32 Hz .

The reciprocity check was carried out by comparing the secondary magnetic fields H_z^s and H_x^s , due to magnetic dipole sources M_x and M_z , respectively, in their reciprocal positions over the same model and frequency. For both the real and imaginary parts of the solution the magnetic field, H_x^s due to the dipole source M_z shows slightly larger peak anomalies; nevertheless, the overall reciprocity check is reasonably good.

The analog results for the tank model were obtained at frequencies of 32 and 263 Hz. These results are shown in Figure 5 along with the corresponding numerical solutions. The results at 32 Hz, especially for the quadrature part, are almost identical and there is a small difference of a few parts per million in the real part. The result at 263 Hz shows excellent agreement for the real part. The quadrature part of the numerical solution, however, shows the peak anomaly about 15 percent less than that of the analog result. The good result for the real part at this frequency is an encouraging sign for the numerical code developed here because as the frequency increases further, the real part of the solution will dominate over the quadrature part.

CONCLUSION

The computer program requires 5.2 megabytes (MB) of memory on the CDC 7600 computer and takes approximately 4 minutes for the finite-element part and 5 minutes for the integration of Green's functions to obtain magnetic fields. The same program requires only 2.8 MB of memory on the IBM 3081 due to the smaller word size (32 bit), but the computation time increases by a factor of 2. Typical computing costs are \$65.00 on the CDC 7600 and \$41.00 on the IBM 3081. The machine precision of the IBM 3081 is 6 to 7 digits, but no significant difference has been observed in the result when compared to the one obtained from the CDC 7600, whose precision is 13 to 14 digits.

Although the flexibility of the finite-element method for representing arbitrary conductivity distributions is lost when using the integral approach, the algorithm still provides ways of analyzing and understanding some of the geophysical problems. The program developed for the study can be more useful with additional sources of finite extent, such as a grounded electric dipole or a large loop, if implemented. If the integral over scattering currents in the entire half-space were used, the computing costs would become prohibitive because of the time-consuming operation of the Green's function integrations. If only quadrature response is required, it appears that satisfactory results can be obtained for half-spaces of arbitrary conductivity distribution using the numerical curl operation, especially if the calculation point is above the interface. If the complete response is required, the conductivity inhomogeneity must be confined to some reasonably compact subvolume of the finite-element mesh to keep the computation within bounds.

Even in the latter case, the conductivity inhomogeneity cannot be too close to the field computation point. For example, the program cannot be used for computation of fields on the surface if the inhomogeneity is close to the surface near the computation point.

ACKNOWLEDGMENTS

This research was supported in part through U.S. Department of Energy contract no. DE-AC03-76SF00098 by the Assistant Secretary for Conservation and Renewable Energy,

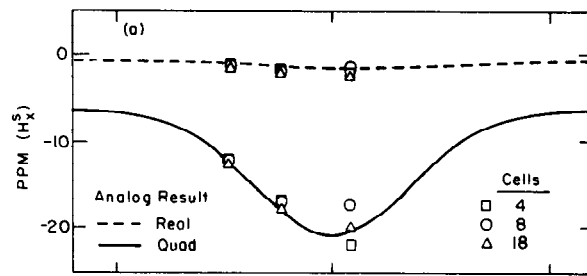


FIG. 4a. Convergence test of the numerical solution. The abscissa represents the location of the array center with respect to the center of the body. The ordinates are in parts per million (ppm) to the free space field.

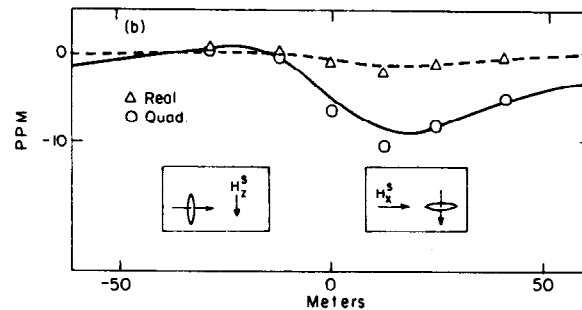


FIG. 4b. Reciprocity check between numerical solutions. The abscissa represents the location of the array center with respect to the center of the body. The ordinates are in parts per million (ppm) to the free space field. The broken and solid lines represent real and quadrature parts of H_z^s due to a horizontal dipole source, respectively. The symbols represent H_x^s due to a vertical dipole at reciprocal positions.

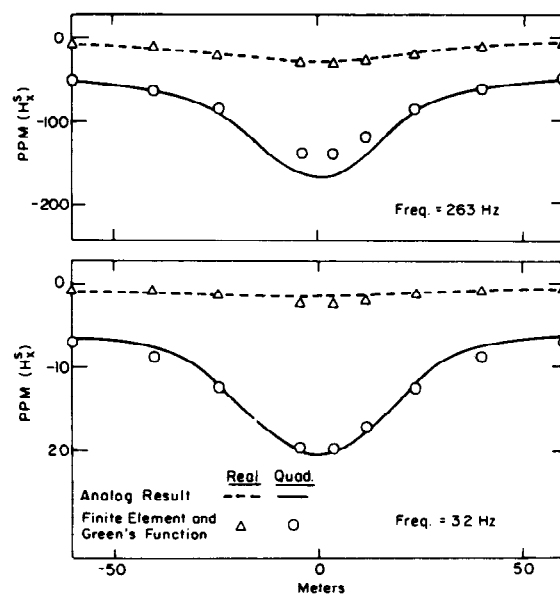


FIG. 5. Comparison between analog result and numerical result with the use of Green's function.

Office of Renewable Technology, Division of Geothermal and Hydropower Technologies. The final phase of the research was conducted with the support of a group of minerals and petroleum industries: Anaconda Copper Co., ARCO Oil and Gas Co., Chevron Resources Co., Exxon Minerals Co., Mobil R & D Corp., Noranda Exploration Inc., and Sohio Petroleum Co., through the University of California, Berkeley.

The authors would like to acknowledge Dr. Michael Hoversten for his contribution to the development of a part of the computer codes while he was with the University of California, Berkeley.

REFERENCES

- Annan, P., 1974, The equivalent source method for electromagnetic scattering analysis and its geophysical application: Ph.D. thesis, Memorial Univ. of Newfoundland.
- Coggon, J. H., 1971, Electromagnetic and electrical modeling by the finite element method: *Geophysics*, **36**, 132-155.
- Hanneson, J. E., 1981, The horizontal loop EM response of a thin vertical conductor in a conductive half-space: Ph.D. thesis, Univ. of Manitoba.
- Harrington, R. F., 1961, Time-harmonic electromagnetic fields: McGraw-Hill Book Co.
- Hohmann, G. W., 1975, Three-dimensional induced polarization and electromagnetic modeling: *Geophysics*, **35**, 901-915.
- Lajoie, J. J., and West, G. F., 1976, The electromagnetic response of a conductive inhomogeneity in a layered earth: *Geophysics*, **41**, 1133-1156.
- Lee, K. H., 1978, Electromagnetic scattering by a two-dimensional inhomogeneity due to an oscillating magnetic dipole: Ph.D. thesis, Univ. of California, Berkeley.
- Lee, K. H., Pridmore, D. F., and Morrison, H. F., 1981, A hybrid three-dimensional electromagnetic modeling scheme: *Geophysics*, **46**, 796-805.
- Meyer, W. H., 1977, Computer modeling of electromagnetic prospecting methods: Ph.D. thesis, Univ. of California, Berkeley.
- Morse, P. M., and Feshbach, H., 1953, *Methods of theoretical physics*: McGraw-Hill Book Co.
- Pridmore, D. F., 1978, Three dimensional modeling of electric and electromagnetic data using the finite element method: Ph.D. thesis, Univ. of Utah.
- Reid, J. K., 1972, Two Fortran subroutines for direct solution of linear equations whose matrix is sparse, symmetric and positive-definite: U.K.A.E.A. Research Group Rep., Harwell, AERE-R7119.
- Ryu, J., 1971, Low frequency electromagnetic scattering: Ph.D. thesis, Univ. of California, Berkeley.
- Stoyer, C. H., and Greenfield, R. J., 1976, Numerical solutions of the response of a two-dimensional earth to an oscillating magnetic dipole source: *Geophysics*, **41**, 519-530.
- Stratton, J. A., 1941, *Electromagnetic theory*: McGraw-Hill Book Co.
- Ward, S. H., 1980, Electrical, electromagnetic and magnetotelluric methods: *Geophysics*, **45**, 1659-1666.
- Weidelt, P., 1975, Electromagnetic induction in three-dimensional structures: *J. Geophys.*, **41**, 85-109.
- , 1981, Dipolinduktion in einer dunnen Platte mit leitfahiger Umgebung und Deckschicht. (Dipole induction by a thin plate in a conductive half-space with an overburden): Federal Inst. for Earth Sciences and Raw Materials, Hannover, Res. Proj. NTS 83 (BMFT), no. 89727.
- Zienkiewicz, O. C., 1977, *The finite element method in engineering science*: McGraw-Hill Book Co.